Article

Millimeter-Scale Unipolar Transport in High Sensitivity Organic-Inorganic Semiconductor X-Ray Detectors

K. D. G. Imalka Jayawardena, Hashini M. Thirimanne, Sandro Francesco Tedde, Judith E. Huerdler, Andrew J. Parnell, R. M. Indrachapa Bandara, Christopher A. Mills, and S. Ravi P. Silva

ACS Nano, **Just Accepted Manuscript** • DOI: 10.1021/acsnano.9b01916 • Publication Date (Web): 24 May 2019

Millimeter-Scale Unipolar Transport in High Sensitivity Organic-Inorganic Semiconductor X-Ray Detectors

*K. D. G. Imalka Jayawardena[1†], Hashini M. Thirimanne[1†], Sandro Francesco Tedde[2], Judith E. Huerdler[2], Andrew J. Parnell[3], R. M. Indrachapa Bandara[1], Christopher A. Mills[1], S. Ravi P. Silva[1]**

1. Advanced Technology Institute, Department of Electrical and Electronic Engineering, University of Surrey, Guildford, Surrey, GU2 7XH, United Kingdom.

2. Siemens Healthineers, Technology Center, Guenther-Scharowsky-Str. 1, 91058 Erlangen, Germany.

3. Department of Physics and Astronomy, University of Sheffield, Hicks Building, Sheffield, S3 7RH, United Kingdom.

Corresponding Author

*E-mail: s.silva@surrey.ac.uk

† These authors contributed equally.

ABSTRACT

Hybrid inorganic-in-organic semiconductors are an attractive class of materials for optoelectronic applications. Traditionally, the thicknesses of organic semiconductors are kept below 1 micron due to poor charge transport in such systems. However, recent work suggests that charge carriers in such organic semiconductors can be transported over centimeter length scales opposing this view. In this work, a unipolar X-ray photoconductor based on a bulk heterojunction architecture, consisting of poly(3-hexylthiophene), a C70 derivative and high atomic number bismuth oxide nanoparticles operating in the 0.1 – 1 mm thickness regime is demonstrated, having a high sensitivity of ~160 $\mu C m Gy^{-1} cm^{-3}$. The high performance enabled by hole drift lengths approaching a millimeter facilitates a

device architecture allowing a high fraction of the incident X-rays to be attenuated. An X-ray imager is demonstrated with sufficient resolution for security applications such as portable baggage screening at border crossings and public events and scalable medical applications.

KEYWORDS

detectors, direct conversion, radiation, inorganics, organics

Due to their low cost and solution processible nature, organic semiconductors based on conjugated polymers and small molecules have been proposed for energy harvesting

applications,[1-3] light emitting devices.[4] In addition to the applications highlighted above, organic semiconductor based devices as well as inorganic-organic hybrid devices are gaining attention for the detection of ionizing radiation.[5,6] The first reported inorganic nanomaterials used for sensitization of organic semiconductor devices for ionizing radiation can be traced to the work of Intaniwet *et al.*[7] where bismuth oxide nanoparticles (Bi_2O_3 NPs) were incorporated into a *p*-type poly(triaryl amine) matrix for detection of ionizing radiation based on a mono-carrier device architecture. The versatility of the concept was further examined through variation of the high atomic number (Z) NP and the organic semiconductor used.[8] In addition to the above developments, Büchele *et al.*[6] demonstrated that the incorporation of gadolinium oxysulfide micro-particles into an organic bulk heterojunction matrix consisting of poly(3-hexythiophene) (P3HT) and [6,6] - Phenyl-C71-butyric acid methyl ester (PCBM) can result in X-ray detector that enable higher resolution imaging capabilities for medical applications extending beyond the current market offerings based on amorphous silicon photodiodes coupled with a cesium iodide scintillator. The importance of the hybrid inorganic-organic semiconductor systems have also been exemplified in the recent work of Civatti *et al.*[9] where the X-ray sensitivity

of a previously demonstrated 6,13-bis(triisopropylsilylethynyl)pentacene system[10] was enhanced by substitution of the silicon atom in organic semiconductor with germanium. In addition to the above, there has also been significant interest in the utilization of perovskite semiconductors as direct conversion ionization radiation detectors[11-13] due to their high X-ray attenuation (as a result of their high average atomics numbers) and high carrier mobilities that enable efficient charge extraction from thick devices (several hundred of microns to millimeters) that is a pre-requisite to enable a fraction of the incident X-rays to be attenuated.

Based on the insights from above developments, we reported a direct conversion X-ray detector concept based on a ternary system comprising of P3HT, PCBM and Bi_2O_3 NPs.[5] Unlike conventional hybrid device concepts where organic semiconductors are utilized for detection of visible – near infrared photons, this device architecture utilized P3HT and PCBM as carrier selective charge transport pathways for free carriers generated due to the interaction between the X-rays and the Bi_2O_3 NPs. This enabled a number of benefits including high X-ray sensitivities of ~1.7 $mCmGy^{-1}cm^{-3}$ when irradiated using “soft” X-rays and ~30 $\mu C\ mGy^{-1}cm^{-3}$ under 6 MV “hard” X-rays. However, the thickness of the

devices were limited to < 30 μm due to the limitations in the fabrication process used as well as due to the prevailing state of knowledge (during the period over which the work was carried out) on the inability for organic semiconductors to transport charge over several hundreds of microns. The high sensitivity obtained with such thin films has critical implications including: a much lower dose detectability which is of importance in dosimetry (*e.g.*: assessing damage to regions surrounding the area of interest in radiotherapy). However, the thin nature and the resulting low attenuation of X-rays has significant negative impact for X-ray imaging where a high X-ray attenuation is required for improving image quality.

Recently, Gélinas *et al.* has shown that photo-generated electrons and holes in organic semiconductors are efficiently separated through delocalized states on the femtosecond time scale[14] which results in the performances typically observed for organic photovoltaics. Furthermore, Burlingame *et al.* demonstrated that the resulting free carriers generated can be transported over centimeter length scales,[15] challenging previously held views of short charge transport lengths in these systems. Such long transport lengths are particularly attractive, especially in terms of the development of ionizing radiation

detectors where thick absorbers are preferred for maximum radiation attenuation.[5,6] Here, a highly sensitive X-ray photoconductor based on the integration of inorganic nanoparticles in an organic bulk heterojunction matrix with hole drift lengths approaching 1 mm is demonstrated. These drift lengths which exceed those of organic single crystals,[16] enables photoconductor thicknesses approaching a millimeter and X-ray sensitivities of ~160 $\mu CmGy^{-1}cm^{-3}$.

RESULTS & DISCUSSION

Dose rate and thickness dependency of X-ray photocurrent response

The X-ray photoconductor developed in this work is based on P3HT as a *p*-type semiconductor, PCBM as an electron trap and Bi_2O_3 NPs as the X-ray attenuator and a route for free carrier generation (Figure 1a). The use of PCBM as an electron transporter, as detailed in our previous work[5] was avoided due to the lower electron mobilities generally observed in fullerene systems.[17] The photoconductor device was completed by deposition of hole-selective gold contacts[18] (Figure 1b,c) resulting in the formation of a

strong Schottky barrier for electrons. Our preliminary investigations focused on a P3HT: PCBM: Bi_2O_3 weight ratio of 1:1:1 which within a photodiode architecture demonstrated a sensitivity of ~1 $mCmGy^{-1}cm^{-3}$. Initially, a photoconductor with a thickness of ~180 μm was fabricated and the X-ray photocurrent response was tested under a 70 kVp X-ray source (Figure S1) with varying X-ray dose rate (*D*) from 20 μGys^{-1} to ~ 1 $mGys^{-1}$ over an X-ray exposure duration of 7 s (Figure 1d) resulting in cumulative exposure doses of 0.14 - 7.5 mGy. The device demonstrated slow rise and decay behavior commensurate with photo conducting characteristics. The X-ray sensitivity (*S*) was evaluated based on[5]

$$S = \frac{1}{D \times T_{X-ray} \times V} \int_0^{T_{X-ray}} \Delta I_{X-ray} dt \quad (1)$$

where $\Delta I_{X\text{-}ray}$ is the X-ray generated photocurrent over a duration of $T_{X\text{-}ray}$ over which the X-ray exposure was carried out and V is the detector volume. A high sensitivity of ~160 $\mu CmGy^{-1}cm^{-3}$ under an applied bias of 200 V was achieved, corresponding to an electric field (*E*) of ~1.2 $V\mu m^{-1}$. These values are a significant improvement over those observed for single crystal organic X-ray detectors[19] and compete with recent reports on single

crystal organic and perovskite X-ray detectors (Figure S2). The mobility-time constant ($\mu\tau$) for the above photoconductors were evaluated using the Hecht equation[11]

$$Q = \frac{Q_0 \mu\tau V}{d^2}\left[1 - exp\left(-\frac{d^2}{\mu\tau V}\right)\right] \quad (2)$$

where Q is the collected charge, Q_0 is the generated charge and d is the detector thickness. Fitting the above relationship to the Q~V characteristics, a $\mu\tau$ constant of ~ 1.7×10^{-6} cm^2V^{-1} was obtained. This is within two orders of magnitude of the values reported for printable perovskite X-ray detectors ($\mu\tau$ = 1 $\times10^{-4}$ cm^2V^{-1})[13] and chlorine doped cadmium telluride single crystals ($\mu\tau$ = 7 $\times10^{-5}$ cm^2V^{-1}).[20] Based on the above $\mu\tau$ values, we estimate a hole drift length (L) of 170 μm. based on $L = \mu\tau E$ (for E = 1 $Vμm^{-1}$), which is on the same length scale as the detector thickness used for the above described photoconductor. This consolidates our understanding of the improved detector performance and rationale for their sensitivity.

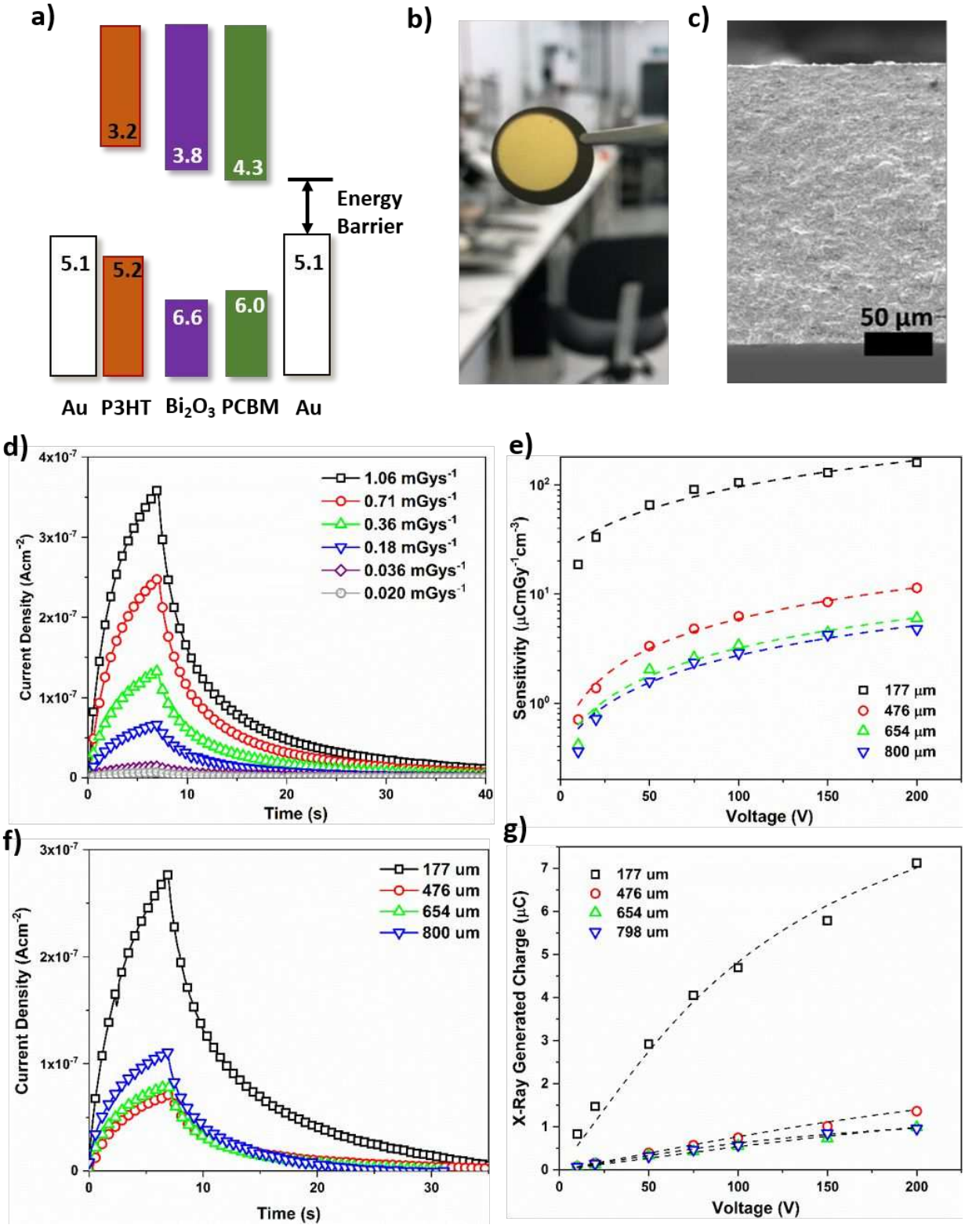
a)
3.2
3.8
4.3
Energy Barrier
5.1
5.2
6.6
6.0
5.1
Au
P3HT
Bi_2O_3
PCBM
Au
b)
c)
50 µm
d)
Current Density (Acm^{-2})
Time (s)
1.06 mGys^{-1}
0.71 mGys^{-1}
0.36 mGys^{-1}
0.18 mGys^{-1}
0.036 mGys^{-1}
0.020 mGys^{-1}
e)
Sensitivity (µCmGy^{-1}cm^{-3})
Voltage (V)
177 µm
476 µm
654 µm
800 µm
f)
Current Density (Acm^{-2})
Time (s)
177 um
476 um
654 um
800 um
g)
X-Ray Generated Charge (µC)
Voltage (V)
177 um
476 um
654 um
798 um

Figure 1. a) The flat band diagram for the different semiconductor materials. All energy values are given in eV. b) Photograph of a fabricated X-ray detector and c) cross sectional scanning electron micrograph of a detector. d) X-ray photocurrent transients under an applied bias of 20 V and different dose rates over a 7 s exposure window. e) Variation in the detector sensitivity under a range of applied voltages for different photoconductor thicknesses, f) example transients under an electric field of 0.2 – 0.3 Vμm^{-1} for different photoconductor thicknesses and g) the Hecht fits for different photoconductor thicknesses.

The fraction of X-rays stopped within the active volume of the detector (F) is given by[21]

$$F = 1 - \exp\left(-\mu_m \rho d\right) \quad (3)$$

where μ_m is the mass attenuation coefficient for a material of density ρ and thickness d. Therefore, increasing the photoconductor thickness and/or its mass attenuation coefficient enables a higher attenuation to be achieved. However, this can only be effective if the entire detector active volume is depleted, with minimal additional

recombination centers which reduce the generated charge components. In view of the exceptionally high carrier transport lengths observed, we first proceeded to investigate the X-Ray photocurrent response of the P3HT:PCBM:Bi_2O_3 (1:1:1) system by increasing the photoconductor thickness up to ~1 mm. Even under such high thickness, not reported previously for P3HT and PCBM based organic semiconductor devices, sensitivities of ~ 5 $\mu CmGy^{-1}cm^{-3}$ are obtained which are still competitive with the more recently reported perovskite based X-ray detectors.[11] In order to ascertain the charge extraction capabilities with increasing thickness, the $\mu\tau$ product was evaluated based on Hecht fits (Figure 1g) which leads to values of 5×10^{-6} cm^2V^{-1} (d = 476 μm), 9×10-6 cm^2V^{-1} (d = 654 μm) and 2.5×10^{-5} cm^2V^{-1} (d = 798 μm). The hole drift lengths, calculated based on the electric field at E = 1.2 $V\mu m^{-1}$, leads to an improvement in the carrier drift lengths with increasing thickness resulting in values of ~1 mm. Such high drift lengths under low electric fields are extremely beneficial in order to extract charges from detectors whose thicknesses lie in the 100 μm – 1 mm length scale (which enables device architectures allowing a higher fraction of incident X-rays to be attenuated and subsequently to be collected).

The carrier transport length scales are significantly higher than those commonly employed for organic photovoltaics, where the thickness is normally restricted to < 300 nm,[22,23] and for organic photodetectors,[24,25] where the thickness is constrained to be < 1 μm to minimize recombination losses. On the other hand, the high drift lengths observed here strongly support recent work by Gelinas *et al.*,[14] where the charge separation at the *p*-type organic semiconductor and *n*-type fullerene interface was driven through delocalized states within the fullerene resulting in charge separation on a very short timescale of 40 fs. While previous work has shown that photo generated electrons can be transported over centimeter length scales, such large transport lengths have, so far, not been utilized in an electronic device resulting in superior device performance. The ability to achieve long charge transport lengths that approach millimeter length scales enables the possibility to fabricate 100 μm – 1 mm thick, high sensitivity X-ray sensors based on a combination of low cost organic semiconductors and high Z nanoparticles with very little or no dead volume within the detector.

Impact of nanoparticle loading on X-ray photocurrent response

Following the improvement in photoconductor thickness, we then proceeded to improve the X-ray stopping power by further increasing the NP loading which in turn improves μ_m. This, in combination with increased detector thickness, could potentially allow for almost 100% attenuation of the incident X-ray photons thereby resulting in high sensitivities. Simulation of the μ_m using NIST XCOM[26] (Figure 2a) for P3HT:PCBM:Bi_2O_3, where the Bi_2O_3 NP loading is varied as 1:1:1, 1:1:2, 1:1:8 and 1:1:16, indicates an increase in μ_m by ~×10. This correspondingly reduces the X-ray attenuation length (*i.e.* the thickness over which 63% of the incident X-rays are stopped) by an equivalent factor. (Figure 2a) Under a bias voltage of – 20 V, increasing the NP loading results in a non-linear decrease of the X-ray sensitivity from a high value of ~40 $\mu CmGy^{-1}cm^{-3}$ for 1:1:1 loading, to < 40 $\mu CmGy^{-1}cm^{-3}$ for higher NP loadings (Figure 2b). The reduced sensitivity despite the increase in the NP loading points towards a disruption in the hole transport properties within the photo conducting layer. This is indicative of a bottleneck in terms of the optimum nanoparticle loading that enables sufficient attenuation of incident X-rays, together with sufficient crystallinity within the charge transporting organic semiconductors to enable high X-ray photocurrents to be realized. The above observations are further supported by

reduction in the μτ product, based on Hecht fits (Figure 2c), which decrease from 1.7×10^{-6} cm^2V^{-1} to 2×10^{-8} cm^2V^{-1} when increasing the NP loading from 1:1:1 to 1:1:16. This is suggestive of a potential limit in NP loading when designing NP sensitized organic-inorganic hybrid detectors, especially at higher thickness (>50 μm).

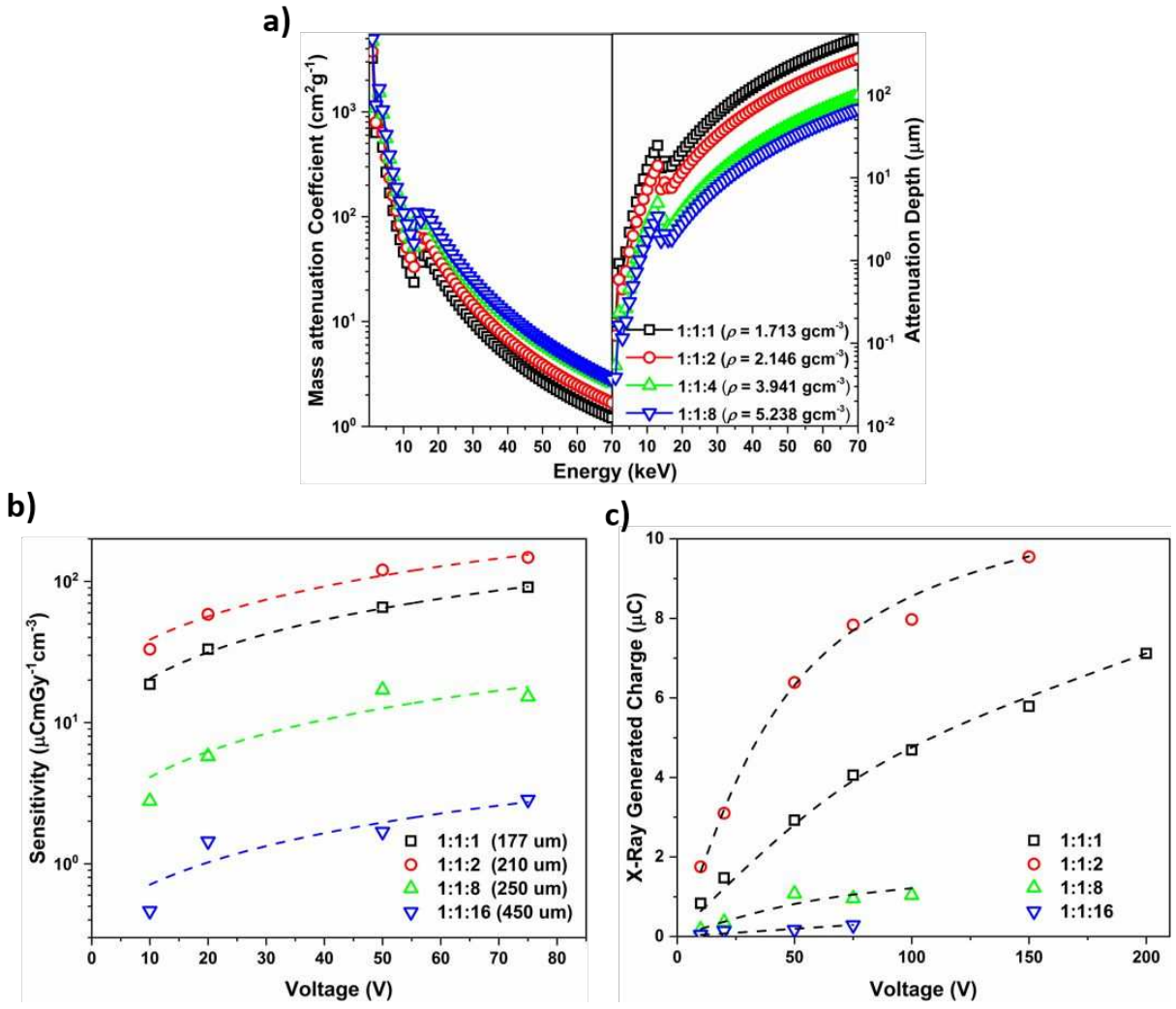

Figure 2. X-ray attenuation and response characteristics under different Bi_2O_3 loadings. a) The variation of the mass attenuation coefficient (left) and attenuation depth (right) , b) X-ray sensitivity and c) X-ray generated charges under applied bias with Hecht fits for P3HT:PCBM:Bi_2O_3 photoconductors for 1:1:1, 1:1:2, 1:1:8 and 1:1:16 ratios.

Impact of nanoparticle loading on the organic semiconductor crystallinity

One of the dominant structural properties that affect the performance of such detectors is the crystallinity of the organic semiconductor systems used. In the case of the detector architecture utilized in this work, achieving a high crystallinity for the P3HT phase is preferable as this would have direct impact on the charge transport properties.[5] In order to observe the impact of the NP loading on the crystallinity of the P3HT, we carried out grazing incidence wide angle x-ray scattering (GIWAXS) measurements on pressed pellets (Figure 3a) and analyzed the evolution of the X-ray scattering peaks for the P3HT, PCBM and Bi_2O_3 NP phases (Figure 3a). Based on the X-ray scattering spectra, it is evident that increasing the P3HT:PCBM:Bi_2O_3 ratio from 1:1:1 to 1:1:2 results in a decrease in intensity for the scattering peaks related to the P3HT phase ((100) and (200)

planes))[5] while these peaks are not observed for the higher NP loadings of 1:1:8 and 1:1:16. The higher intensities observed for the (100) plane of P3HT indicates that despite the powder nature of the starting material, P3HT has a more preferential "edge on" orientation where the P3HT lamellar align parallel to the planar surface of the pellet with the side chains oriented perpendicular to the planar pellet surface. With regards to the PCBM, we note that a noticeable scattering peak is unobservable. This is attributed to the GIWAXS spectra being strongly dominated by the scatter peaks due to the Bi_2O_3 NPs resulting in weakly scattering peaks (such as those due to the PCBM phase) to be unobservable. The observation of sharp peaks in the GIWAXS spectra for the Bi_2O_3 NPs are in agreement with the crystalline nature of this material whose characteristics based on X-ray powder diffraction studies were reported previously.[5] In order to verify that the loss of crystallinity is not due to the fabrication methodology utilized, we carried out differential scanning calorimetry (DSC) on the P3HT:PCBM:Bi_2O_3 starting powders used for the fabrication of the pellets (Figure S3).[20] DSC analysis for the P3HT phase in P3HT:PCBM:Bi_2O_3 samples at ratios of 1:1:1 and 1:1:2 shows crystallinity of around 5-6%. On the other hand, the crystallinity of P3HT is well below the limits that can be

observed for the 1:1:8 and 1:1:16 systems which is in agreement with the observations made from the GIWAXS analysis. The loss in crystallinity for the P3HT phase which in the detector architecture utilized here explains the poor sensitivity and $\mu\tau$ constants for the 1:1:8 and 1:1:16 samples where the charge extraction is inhibited due to the more disordered nature of the hole transporting P3HT phase.

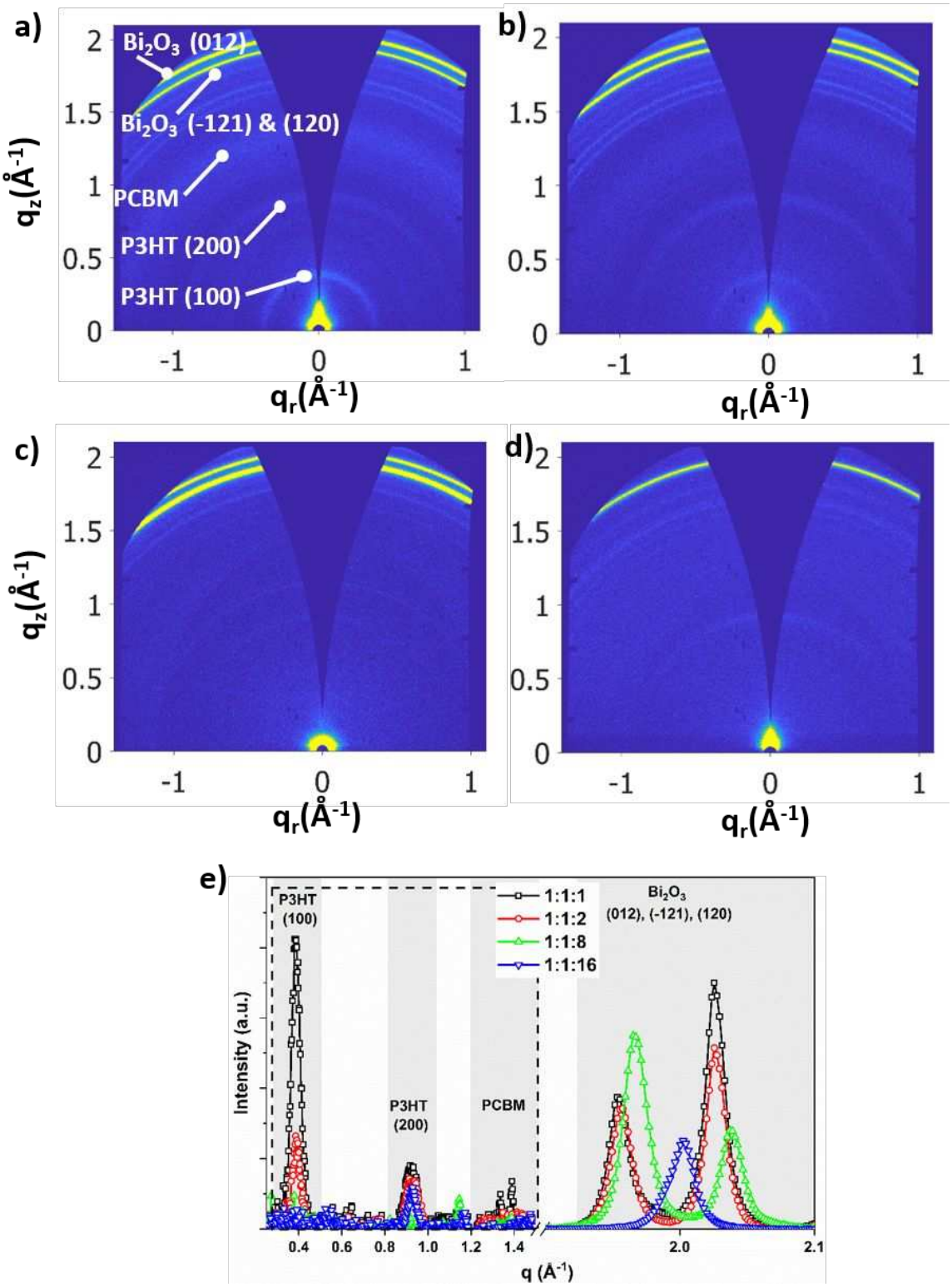
a)
b)
c)
d)
e)
Bi_2O_3 (012)
Bi_2O_3 (-121) & (120)
PCBM
P3HT (200)
P3HT (100)
q_z(Å^{-1})
q_r(Å^{-1})
1:1:1
1:1:2
1:1:8
1:1:16
Bi_2O_3 (012), (-121), (120)
Intensity (a.u.)
q (Å^{-1})

Figure 3. 2D GIWAXS spectra for the hybrid pellets based on P3HT:PCBM:Bi_2O_3 NP ratios of a) 1:1:1, b) 1:1:2, c) 1:1:8 and d) 1:1:16. e) 1D spectra extracted from the 2D GIWAXS plots. A noticeable decrease in the peak intensities for the (100) and (200) P3HT crystalline planes are observed for 1:1:8 and 1:1:16 samples indicating loss of P3HT crystallinity while scatter peaks for the PCBM phase are not observable due to the high scattering intensities of the Bi_2O_3 NPs. The X-ray scattering intensities in the range of q = 0.2 – 1.5 $Å^{-1}$ (indicated by the dashed box) have been scaled by x30.

X-ray imaging characteristics

Finally, we proceeded to fabricate an X-ray imager (Figure 4a) based on the best performing P3HT:PCBM:Bi_2O_3 1:1:1 loading condition at a detector thickness of ~250 μm. For the fabrication of an array of detector pixels, for imaging purposes, the photo conducting wafer was interfaced by contacting an array of thin film transistors (Figure 4b), The spatial resolution of the detector was determined using the modulation transfer function (MTF) (Figure 4e) *via* the slanted edge method. The MTF of the

P3HT:PCBM:Bi_2O_3 based imager possesses a value of 0.2 at ~1 $lpmm^{-1}$ which is suitable for applications where millimeter to submillimeter scale features require to be discriminated as in for example, baggage scanning in border security. Therefore, we envisage these photoconductors to be used for X-ray imaging in security applications where the feature sizes of the objects observed are larger than several millimeters.

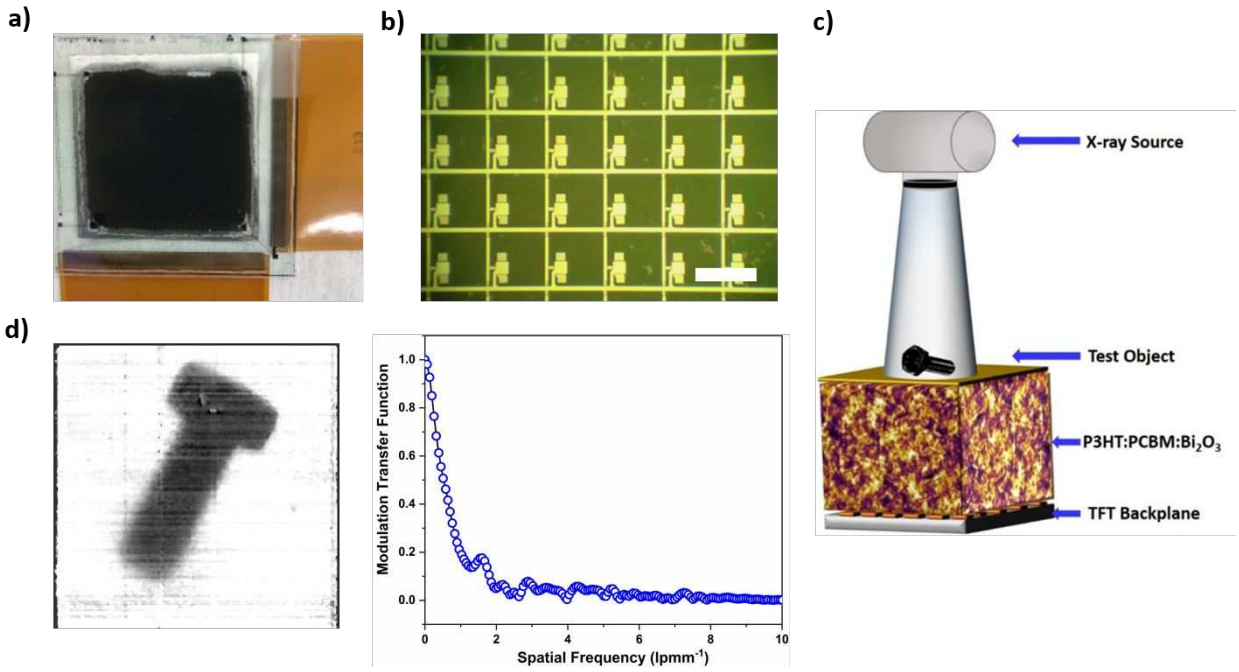

Figure 4. X-ray imager characteristics. a) photograph of the 1st generation imager prepared using a ratio of 1:1:1 P3HT:PCBM:Bi_2O_3, and detector thickness of 250 µm. b) photograph of pixelated array where each pixel is addressed by a transistor (scale bar = 100 µm). c) schematic of the imager architecture where the individual pixels are

addressed using a matrix of transistors as shown in b). d) X-ray image of a screw obtained using the imager and e) the MTF of the imager as obtained based on the slanted edge method.

Avenues for future developments

While the detector architecture developed in this work shows promise for dosimetry and imaging applications, further developments of several key parameters are required in order for this architecture to be truly competitive with existing commercial technologies. The rise and decay times of the devices presented here (as evident in the transient X-ray photocurrent responses given in Figures 1d,f) proceeds over several seconds. This is in contrast to commercial detector materials such as those based on the combination of cesium iodide scintillators and amorphous silicon photodiodes which have been optimized to obtain > 10 frames per second,[27] diamond single crystals[28] (rise and fall times of ~1.1 s and ~0.4 s, the latter limited by measurement apparatus used) as well as cadmium zinc telluride single crystals (rise and fall times < 100 ns).[29] As the rise and decay times are often a reflection of the charge trapping and de-trapping processes taking place within

the relatively disordered organic semiconductor matrix (in comparison to its inorganic counterparts), we speculate that the replacement of the current organic semiconductors or inclusion of a inorganic material possessing higher carrier mobilities are likely to lead to significant improvement in the response times. Potential solution processible high mobility semiconductors includes organic semiconductors developed for organic thin film transistor applications such as 6,13-bis(triisopropylsilylethynyl)[30] or poly[4-(4,4-dihexadecyl-4H-cyclopenta[1,2-b:5,4-b′]dithiophen-2-yl)-alt-[1,2,5]-thiadiazolo[3,4-c]pyridine].[31]

The second key factor that affects the performance of the detector architecture developed for both dosimetry and imaging is the high pixel dark currents observed (Figure S4) which leads to a signal to noise ratio < 0.2. This in turn results in images that display very low contrast (as visually evident from Figure 4d) as well as limit the dynamic range of the detector. Among organic semiconductors used for organic photodiode applications (including for indirect radiation detection), P3HT has been observed to result in high dark currents.[6] On the other hand, *p*-type organic semiconductors such as poly[N-9′-heptadecanyl-2,7-carbazole-alt-5,5-(4′,7′-di-2-thienyl-2′,1′,3′-benzothiadiazole)] as well

as several other non-disclosed polymers have been reported to result in dark currents < 1 $nAcm^{-2}$ [32,33] approaching the performance of amorphous silicon photodiodes. Replacement of the current P3HT system with the above *p*-type semiconductors is more than likely to enable the detector dark current to be reduced to an industry acceptable level of 0.1 $nAcm^{-2}$.

CONCLUSION

In conclusion, we have demonstrated hole drift lengths in P3HT:PCBM:Bi_2O_3 heterojunction architectures exceeding 100 μm, where the PCBM phase acts as an electron trap enabling hole only device behavior. The high hole transport lengths enable thick P3HT:PCBM:Bi_2O_3 device fabrication for high X-ray attenuation resulting in a best X-ray sensitivity of ~160 $\mu CmGy^{-1}cm^{-3}$. Based on the above, the possibility of increasing the X-ray attenuation through increased nanoparticle loading was investigated. However, a noticeable decrease in the X-ray sensitivity was observed. Structural studies carried out based on varying nanoparticle loading suggests that the increased nanoparticle length leads to a loss in P3HT crystallinity which results in the degradation of the X-ray

photocurrent response, hence indicating the importance of an optimized nanoparticle loading for such hybrid “inorganics-in-organics” materials. Based on the above observations, a prototype imager was developed combining the P3HT:PCBM:Bi_2O_3 X-ray photoconductor with an a-Si backplane. The resulting imager demonstrates an MTF value of ~ 1 $lpmm^{-1}$ which indicates the possibility of resolving features in the millimeter length scales with potential applications such as in dose mapping for radiotherapy, scanning at border control. However, there still exists several key characteristics features such as the reduction of dark current, improving rise and decay times that would enable systems to be utilized for dynamic X-ray imaging. Such developments are expected through developments in organic semiconductors with high mobilities, which in combination with the characteristics developed here are expected to enable a broad range of applications.

MATERIALS AND METHODS

Powder preparation. Regioregular P3HT (Rieke) and PCBM (Solenne) where added to anhydrous chloroform at concentrations of 80 $mgml^{-1}$ each and left to stir overnight. Bi_2O_3 nanopowder with an average particle size of 38 nm was added to form P3HT:PCBM:Bi_2O_3 mixtures with weight loadings as described. The mixture was left to stir overnight. Addition of the organic semiconductors and the Bi_2O_3 nanopowder was carried out in a N_2 glove box (MBraun) with O_2 and H_2O content of < 1 ppm. For precipitation of the powders, 1 ml of ethanol was added to 1 ml of the starting solution and then rotary evaporated. The dried powder was then further dried under vacuum overnight to remove any residual solvent.

Wafer and detector preparation. A hydraulic press (Perkin Elmer FTIR pellet press) with a 15 mm die was used for sintering. A polished stainless-steel cylinder was placed in the bore of the cylinder body by an Al foil. 100–1000 mg of the P3HT:PCBM:Bi_2O_3 powder was then loaded into the bore. Next, a second polished cylinder which is covered by an Al foil and a plunger were inserted into the cylinder body. A 1000 kg load was applied to form the pellet for 15 min with the pellet pressing being carried out at room temperature.

The use of the Al foils enables a visual identification of the smoothness of the pressed pellets. For completion of the photoconductor devices, 100 nm of gold with an overlap area of 1 cm^2 was sputtered through a shadow mask.

X-ray photocurrent response measurement. The X-ray photo response was obtained using a 70 kV X-ray source (Siemens MEGALIX Cat Plus 125/40/90, 124 GW) with a tungsten anode. The X-ray spectrum was filtered with a 2.5-mm-thick Al plate. The dose rate was varied by changing the X-ray tube current with calibrated with a PTW Diados T11003-001896 dosimeter. Electrical readouts where carried out using a Keithley 2400 source measure unit at 100 ms. Image read-out and processing: A 256×256 amorphous silicon thin film transistor panel was used for the imager in conjunction with a commercially available read-out IC (ROIC) (ISC9717 from Flir). The pixel pitch is 98 μm. The input signal was integrated, amplified and subjected to a low pass filter simultaneously and converted from analog to digital using a 14-bit AD converter. The integrator feedback capacitance used was 2 pF and the integration time was 10 ms. Dark images taken with and without the sensor, were used in order to evaluate the noise of the system. Dark

image and flat field correction was carried out to obtain X-ray recordings. The modulation transfer function (MTF) was determined using the slanted-edge method[34] *via* an ImageJ plug-in.

GIWAXS. GIWAXS measurements were performed using a Xeuss 2.0 (XENOCS, France) system equipped with a MetalJet (Excillum, Sweden) liquid gallium source which provides a 9.24 keV X-ray beam. The beam was collimated to a spot of with a lateral dimension of 400 µm on the sample. Pilatus3R 1M 2D detector (Dectris, Switzerland) placed at ~311 mm from the sample was used to obtain the diffraction images. Calibration of the sample=detector distance was carried out using a silver behenate calibrant in transmission geometry while the GIWAXS measurements were carried out at an incident angle of 0.3°. The diffraction images were then remapped from pixel to scattering vector using the software Foxtrot (Soleil France).

ASSOCIATED CONTENT

K.D.G.I.J., H.M.T., C.A.M. & S.R.P.S. have a filed patent (Direct Conversion Radiation Detector, International Publication Number: WO 2018/078372 Al) which is assigned to a startup company (SilverRay Ltd.).

Supporting Information.

The Supporting Information is available free of charge on the ACS Publications website at XXX

The Supporting Information provided consists of additional details regarding the simulated X-ray photon density spectrum, X-ray sensitivity comparison chart, DSC analysis and dark current characteristics.

AUTHOR INFORMATION

Author Contributions

K.D.G.I.J. and H.M.T. conceived the idea and planned the project with additional input from S.F.T and C.A.M; prepared the powder for the fabrication of pellets. J.E.H. fabricated

the pellets and the imager while H.M.T. and S.F.T. carried out the X-ray detector and imager characterization. K.D.G.I.J. analyzed the X-ray photoconductor data while S.F.T. analyzed the measurements from the X-ray imager. A.J.P. carried out the GIWAXS measurements and analyzed the data with contribution from K.D.G.I.J. R.M.I.B. prepared samples for SEM measurements, and for DSC characterization and analyzed the results obtained. C.A.M and S.R.P.S. proposed the project and oversaw the delivery of the project objectives. K.D.G.I.J. drafted the manuscript and compiled the figures. All authors discussed the results and provided feedback on the manuscript.

ACKNOWLEDGMENT

K.D.G.I.J., H.M.T., C.A.M. and S.R.P.S. gratefully acknowledge support for this work from the Leverhulme Trust through research project grant (RPG-2014-312). S.R.P.S. acknowledges EPSRC for funding through research project grant (EP/R025304/1). R.M.I.B. acknowledges support from the University of Surrey Overseas Research Scholarship/University Research Scholarship. The GIWAXS measurements were

performed on the Sheffield Xeuss 2.0 SAXS instrument, A.J.P. is grateful to Xenocs for their ongoing help and support in the user program at the University of Sheffield. We thank V. Doukova (University of Surrey) for providing assistance on obtaining DSC results.

References

(1) Meng, L.; Zhang, Y.; Wan, X.; Li, C.; Zhang, X.; Wang, Y.; Ke, X.; Xiao, Z.; Ding, L.; Xia, R.; Yip, H.-L.; Cao, Y.; Chen, Y. Organic And Solution-Processed Tandem Solar Cells With 17.3% Efficiency. *Science* **2018**, 361, 1094–1098.

(2) Che, X.; Li, Y.; Qu, Y.; Forrest, S. R. High Fabrication Yield Organic Tandem Photovoltaics Combining Vacuum- And Solution-Processed Subcells With 15% Efficiency. *Nat. Energy* **2018**, 3, 422–427.

(3) Jayawardena, K. D. G. I.; Rozanski, L. J.; Mills, C. A.; Beliatis, M. J.; Nismy, N. A.; Silva, S. R. P. 'Inorganics-In-Organics': Recent Developments And Outlook For 4G Polymer Solar Cells. *Nanoscale* **2013**, 5, 8411–8427.

(4) Liu, Y.; Li, C.; Ren, Z.; Yan, S.; Bryce, M. R. All-Organic Thermally Activated Delayed Fluorescence Materials For Organic Light-Emitting Diodes. *Nat. Rev. Mater.* **2018**, 3, 18020.

(5) Thirimanne, H. M.; Jayawardena, K. D. G. I.; Parnell, A. J.; Bandara, R. M. I.; Karalasingam, A.; Pani, S.; Huerdler, J. E.; Lidzey, D. G.; Tedde, S. F.; Nisbet, A.; Mills, C. A.; Silva, S. R. P. High Sensitivity Organic Inorganic Hybrid X-Ray Detectors With Direct Transduction And Broadband Response. *Nat. Commun.* **2018**, 9, 2926.

(6) Büchele, P.; Richter, M.; Tedde, S. F.; Matt, G. J.; Ankah, G. N.; Fischer, R.; Biele, M.; Metzger, W.; Lilliu, S.; Bikondoa, O.; Macdonald, J. E.; Brabec, C. J.; Kraus, T.; Lemmer, U.; Schmidt, O. X-Ray Imaging With Scintillator-Sensitized Hybrid Organic Photodetectors. *Nat. Photonics* **2015**, 9, 843–848.

(7) Intaniwet, A.; Mills, C. A.; Shkunov, M.; Sellin, P. J.; Keddie, J. L. Heavy Metallic Oxide Nanoparticles For Enhanced Sensitivity In Semiconducting Polymer X-Ray Detectors. *Nanotechnology* **2012**, 23, 235502.

(8) Mills, C. A.; Al-Otaibi, H.; Intaniwet, A.; Shkunov, M.; Pani, S.; Keddie, J. L.; Sellin, P. J. Enhanced X-Ray Detection Sensitivity In Semiconducting Polymer Diodes Containing Metallic Nanoparticles. *J. Phys. D. Appl. Phys.* **2013**, 46, 275102.

(9) Ciavatti, A.; Basiricò, L.; Fratelli, I.; Lai, S.; Cosseddu, P.; Bonfiglio, A.; Anthony, J. E.; Fraboni, B. Boosting Direct X-Ray Detection In Organic Thin Films By Small Molecules Tailoring. *Adv. Funct. Mater.* **2018**, 29, 1806119.

(10) Basiricò, L.; Ciavatti, A.; Cramer, T.; Cosseddu, P.; Bonfiglio, A.; Fraboni, B. Direct X-Ray Photoconversion In Flexible Organic Thin Film Devices Operated Below 1 V. *Nat. Commun.* **2016**, 7, 13063.

(11) Shrestha, S.; Fischer, R.; Matt, G. J.; Feldner, P.; Michel, T.; Osvet, A.; Levchuk, I.; Merle, B.; Golkar, S.; Chen, H.; Tedde, S. F.; Schmidt, O.; Hock, R.; Rührig, M.; Göken, M.; Heiss, W.; Anton, G.; Brabec, C. J. High-Performance Direct Conversion X-Ray Detectors Based On Sintered Hybrid Lead Triiodide Perovskite Wafers. *Nat. Photonics* **2017**, 11, 436–440.

(12) He, Y.; Matei, L.; Jung, H. J.; McCall, K. M.; Chen, M.; Stoumpos, C. C.; Liu, Z.; Peters, J. A.; Chung, D. Y.; Wessels, B. W.; Wasielewski, M. R.; Dravid, V. P.; Burger, A.; Kanatzidis, M. G. High Spectral Resolution Of Gamma-Rays At Room Temperature By Perovskite Cspbbr3 Single Crystals. *Nat. Commun.* **2018**, 9, 1609.

(13) Kim, Y. C.; Kim, K. H.; Son, D.-Y.; Jeong, D.-N.; Seo, J.-Y.; Choi, Y. S.; Han, I. T.; Lee, S. Y.; Park, N.-G. Printable Organometallic Perovskite Enables Large-Area, Low-Dose X-Ray Imaging. *Nature* **2017**, 550, 87–91.

(14) Gélinas, S.; Rao, A.; Kumar, A.; Smith, S. L.; Chin, A. W.; Clark, J.; van der Poll, T. S.; Bazan, G. C.; Friend, R. H. Ultrafast Long-Range Charge Separation In Organic Semiconductor Photovoltaic Diodes. *Science* **2014**, 343, 512–516.

(15) Burlingame, Q.; Coburn, C.; Che, X.; Panda, A.; Qu, Y.; Forrest, S. R. Centimetre-Scale Electron Diffusion In Photoactive Organic Heterostructures. *Nature* **2018**, 554, 77–80.

(16) Ciavatti, A.; Capria, E.; Fraleoni-Morgera, A.; Tromba, G.; Dreossi, D.; Sellin, P. J.; Cosseddu, P.; Bonfiglio, A.; Fraboni, B. Toward Low-Voltage And Bendable X-Ray Direct Detectors Based On Organic Semiconducting Single Crystals. *Adv. Mater.* **2015**, 27, 7213–7220.

(17) Armin, A.; Shoaee, S.; Lin, Q.; Burn, P. L.; Meredith, P. On The Unipolarity Of Charge Transport In Methanofullerene Diodes. *npj Flex. Electron.* **2017**, 1, 13.

(18) Dabera, G. D. M. R.; Jayawardena, K. D. G. I.; Prabhath, M. R. R.; Yahya, I.; Tan, Y. Y.; Nismy, N. A.; Shiozawa, H.; Sauer, M.; Ruiz-Soria, G.; Ayala, P.; Stolojan, V.; Adikaari, A. A. D. T.; Jarowski, P. D.; Pichler, T.; Silva, S. R. P. Hybrid Carbon Nanotube Networks As Efficient Hole Extraction Layers For Organic Photovoltaics. *ACS Nano* **2013**, 7, 556–565.

(19) Fraboni, B.; Fraleoni-Morgera, A.; Zaitseva, N. Ionizing Radiation Detectors Based On Solution-Grown Organic Single Crystals. *Adv. Funct. Mater.* **2016**, 26, 2276–2291.

(20) Sellin, P. J.; Davies, A. W.; Lohstroh, A.; Ozsan, M. E.; Parkin, Drift Mobility And Mobility-Lifetime Products In Cdte:Cl Grown By The Travelling Heater Method. J. *IEEE Trans. Nucl. Sci.* **2005**, 52, 3074–3078.

(21) X-Ray Mass Attenuation Coefficients | NIST https://www.nist.gov/pml/x-ray-mass-attenuation-coefficients (accessed Oct 5, 2018).

(22) Park, S. H.; Roy, A.; Beaupré, S.; Cho, S.; Coates, N.; Moon, J. S.; Moses, D.; Leclerc, M.; Lee, K.; Heeger, A. J. Bulk Heterojunction Solar Cells With Internal Quantum Efficiency Approaching 100%. *Nat. Photonics* **2009**, *3*, 297–302.

(23) He, Z.; Xiao, B.; Liu, F.; Wu, H.; Yang, Y.; Xiao, S.; Wang, C.; Russell, T. P.; Cao, Y. Single-Junction Polymer Solar Cells With High Efficiency And Photovoltage. *Nat. Photonics* **2015**, 9, 174–179.

(24) Armin, A.; Hambsch, M.; Kim, I. K.; Burn, P. L.; Meredith, P.; Namdas, E. B. Thick Junction Broadband Organic Photodiodes. *Laser Photon. Rev.* **2014**, 8, 924–932.

(25) Armin, A.; Jansen-van Vuuren, R. D.; Kopidakis, N.; Burn, P. L.; Meredith, P. Narrowband Light Detection *Via* Internal Quantum Efficiency Manipulation Of Organic Photodiodes. *Nat. Commun.* **2015**, 6, 6343.

(26) US Department Of Commerce, NIST XCOM: Photon Cross Sections Database, http://www.nist.gov/pml/data/xcom/, accessed: December, 2018.

(27) Medical Flat Panel Detectors | Varex Imaging https://www.vareximaging.com/products/medical/medical-flat-panel-detectors (accessed Apr 8, 2019).

(28) Abdel-Rahman, M. A. E.; Lohstroh, A.; Jayawardena, I.; Henley, S. J. The X-Ray Detection Performance Of Polycrystalline CVD Diamond With Pulsed Laser Deposited Carbon Electrodes. *Diam. Relat. Mater.* **2012**, 22, 70–76.

(29) Zhao, X. C.; Ouyang, X. P.; Xu, Y. D.; Han, H. T.; Zhang, Z. C.; Wang, T.; Zha, G. Q.; Ouyang, X. Time Response Of Cd0.9Zn0.1Te Crystals Under Transient And Pulsed Irradiation. *AIP Adv.* **2012**, 2, 012162.

(30) Intaniwet, A.; Keddie, J. L.; Shkunov, M.; Sellin, P. J. High Charge-Carrier Mobilities In Blends Of Poly(Triarylamine) And TIPS-Pentacene Leading To Better Performing X-Ray Sensors. *Org. Electron.* **2011**, 12, 1903–1908.

(31) Luo, C.; Kyaw, A. K. K.; Perez, L. A.; Patel, S.; Wang, M.; Grimm, B.; Bazan, G. C.; Kramer, E. J.; Heeger, A. J. General Strategy For Self-Assembly Of Highly Oriented Nanocrystalline Semiconducting Polymers With High Mobility. *Nano Lett.* **2014**, 14, 2764–2771.

(32) Kielar, M.; Dhez, O.; Pecastaings, G.; Curutchet, A.; Hirsch, L. Long-Term Stable Organic Photodetectors With Ultra Low Dark Currents For High Detectivity Applications. *Sci. Rep.* **2016**, 6, 39201.

(33) Gelinck, G. H.; Kumar, A.; Moet, D.; van der Steen, J.-L. P. J.; van Breemen, A. J. J. M.; Shanmugam, S.; Langen, A.; Gilot, J.; Groen, P.; Andriessen, R.; Simon, M.; Ruetten, W.; Douglas, A. U.; Raaijmakers, R.; Malinowski, P. E.; Myny, K. X-Ray Detector-On-Plastic With High Sensitivity Using Low Cost, Solution-Processed Organic Photodiodes. *IEEE Trans. Electron Devices* **2016**, 63, 197–204.

(34) Samei, E.; Flynn, M. J.; Reimann, D. A. A Method For Measuring The Presampled MTF Of Digital Radiographic Systems Using An Edge Test Device. *Med. Phys.* **1998**, 25, 102–113.

(35) Yakunin, S.; Dirin, D. N.; Shynkarenko, Y.; Morad, V.; Cherniukh, I.; Nazarenko, O.; Kreil, D.; Nauser, T.; Kovalenko, M. V. Detection Of Gamma Photons Using Solution-Grown Single Crystals Of Hybrid Lead Halide Perovskites. *Nat. Photonics* **2016**, 10, 585–589.

(36) Mills, C. A.; Intaniwet, A.; Shkunov, M.; Keddie, J. L.; Sellin, P. J. Flexible Radiation Dosimeters Incorporating Semiconducting Polymer Thick Films. *Proc. SPIE*, **2009**, 7449, 74491I.

(37) Intaniwet, A.; Mills, C. A.; Shkunov, M.; Thiem, H.; Keddie, J. L.; Sellin, P. J. Characterization Of Thick Film Poly(Triarylamine) Semiconductor Diodes For Direct X-Ray Detection. *J. Appl. Phys.* **2009**, 106, 064513.

(38) Ankah, G. N.; Büchele, P.; Poulsen, K.; Rauch, T.; Tedde, S. F.; Gimmler, C.; Schmidt, O.; Kraus, T. Pbs Quantum Dot Based Hybrid-Organic Photodetectors For X-Ray Sensing. *Org. Electron.* **2016**, 33, 201–206.

(39) Yakunin, S.; Sytnyk, M.; Kriegner, D.; Shrestha, S.; Richter, M.; Matt, G. J.; Azimi, H.; Brabec, C. J.; Stangl, J.; Kovalenko, M. V.; Heiss, W. Detection Of X-Ray Photons By Solution-Processed Lead Halide Perovskites. *Nat. Photonics* **2015**, 9, 444–449.

(40) Wei, H.; Fang, Y.; Mulligan, P.; Chuirazzi, W.; Fang, H.-H.; Wang, C.; Ecker, B. R.; Gao, Y.; Loi, M. A.; Cao, L.; Huang, J. Sensitive X-Ray Detectors Made Of Methylammonium Lead Tribromide Perovskite Single Crystals. *Nat. Photonics* **2016**, 10, 333–339.

(41) Lai, S.; Cosseddu, P.; Basiricò, L.; Ciavatti, A.; Fraboni, B.; Bonfiglio, A. A Highly Sensitive, Direct X-Ray Detector Based On A Low-Voltage Organic Field-Effect Transistor. *Adv. Electron. Mater.* **2017**, 3, 1600409.

(42) Wei, W.; Zhang, Y.; Xu, Q.; Wei, H.; Fang, Y.; Wang, Q.; Deng, Y.; Li, T.; Gruverman, A.; Cao, L.; Huang, J. Monolithic Integration Of Hybrid Perovskite Single Crystals With Heterogenous Substrate For Highly Sensitive X-Ray Imaging. *Nat. Photonics* **2017**, 11, 315–321.

(43) Pan, W.; Wu, H.; Luo, J.; Deng, Z.; Ge, C.; Chen, C.; Jiang, X.; Yin, W.-J.; Niu, G.; Zhu, L.; Yin, L.; Zhou, Y.; Xie, Q.; Ke, X.; Sui, M.; Tang, J. $Cs_2AgBiBr_6$ Single-Crystal X-Ray Detectors With A Low Detection Limit. *Nat. Photonics* **2017**, 11, 726–732.

(44) Ciavatti, A.; Cramer, T.; Carroli, M.; Basiricò, L.; Fuhrer, R.; De Leeuw, D. M.; Fraboni, B. Dynamics Of Direct X-Ray Detection Processes In High-Z Bi2O3

Nanoparticles-Loaded PFO Polymer-Based Diodes. *Appl. Phys. Lett.* **2017**, 111, 183301.

(45) Kasap, S. O. X-Ray Sensitivity Of Photoconductors: Application To Stabilized a-Se. *J. Phys. D. Appl. Phys.* **2000**, 33, 2853–2865.

(46) Won, J. H.; Kim, K. H.; Suh, J. H.; Cho, S. H.; Cho, P. K.; Hong, J. K.; Kim, S. U. The X-Ray Sensitivity Of Semi-Insulating Polycrystalline Cdznte Thick Films. *Nucl. Instruments Methods Phys. Res. Sect. A Accel. Spectrometers, Detect. Assoc. Equip.* **2008**, 591, 206–208.

(47) Oh, K. M.; kim, D. K.; Shin, J. W.; Heo, S. U.; Kim, J. S.; Park, J. G.; Nam, S. H. Measurement Of The Electrical Properties Of A Polycrystalline Cadmium Telluride For Direct Conversion Flat Panel X-Ray Detector. *J. Instrum.* **2014**, 9, P01010–P01010.

(48) Kingsley, J. W.; Weston, S. J.; Lidzey, D. G. Stability Of X-Ray Detectors Based On Organic Photovoltaic Devices. *IEEE J. Sel. Top. Quantum Electron.* **2010**, 16, 1770–1775.

(49) Schafferhans, J.; Baumann, A.; Wagenpfahl, A.; Deibel, C.; Dyakonov, V. Oxygen Doping Of P3HT:PCBM Blends: Influence On Trap States, Charge Carrier Mobility And Solar Cell Performance. *Org. Electron.* **2010**, 11, 1693–1700.

(50) Bracher, C.; Yi, H.; Scarratt, N. W.; Masters, R.; Pearson, A. J.; Rodenburg, C.; Iraqi, A.; Lidzey, D. G. The Effect Of Residual Palladium Catalyst On The Performance And Stability Of PCDTBT:PC70BM Organic Solar Cells. *Org. Electron.* **2015**, 27, 266–273.

ToC figure

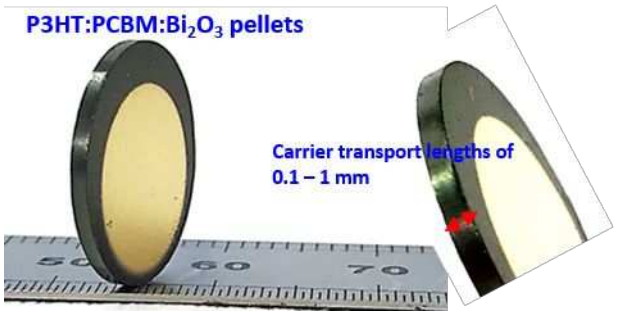
P3HT:PCBM:Bi_2O_3 pellets
Carrier transport lengths of
0.1 – 1 mm